An Investigation of Microclimatological Conditions Along Elevation Transects Near Ithaca, NY

Honors Thesis
Presented to the College of Agriculture and Life Sciences, Physical Sciences division,
Cornell University
in Partial Fulfillment of the Requirements for the
Research Honors Program

by
Colin Raymond
May 2014

Advisor: Professor Art DeGaetano, Earth and Atmospheric Sciences

Abstract

A field campaign was conducted in complex topography near Ithaca, NY with the aim of determining and describing both qualitatively and quantitatively the variables that affect nighttime temperatures there. Observations were compared against a weighted average of nearby private-weather-station readings and Rapid Refresh [RAP]-model gridpoint forecasts for the corresponding time periods. Local nowcasts or forecasts for locations along the transects — generated from a similarity analysis of station and transect-location metadata — showed generally poor skill, though the consistently greater errors at higher elevations suggest the potential for fruitful additional adjustments beyond the scope of this study. A distinct reversal in the upslope wind corresponding to lapse rates near the moist-adiabatic value supports the hypothesis of a triggered hilltop cold-air pool. Nights with strong potential-temperature inversions had remarkably similar synoptic-scale conditions, which bore the hallmarks of a valley inversion being entrained from above by warm southeast winds. Bolstering this hypothesis was the definite linear relationship found between observed lapse rates and region-wide temperature trends on clear nights, but not cloudy ones. To better account for these findings, a new forecast scheme was then implemented, combining regressions of observed along-transect lapse rates on upslope winds, modeled open-sky lapse rates, and region-wide temperature trends; it demonstrated improved skill over the station-based one, suggesting that further work to enable standardization of microclimatic forecasts based on a simple set of externally measured variables would be both possible and productive.

Introduction and Research Questions

A number of studies have examined the patterns of weather conditions in dense urban settings (Georgakis and Santamouris 2006; Niachou et. al. 2008; Sonne and Vieira 2000), while others have conducted measurement trials over vegetated hills and valleys (Froelich and Schmid 2006; Lookingbill and Urban 2003; Pypker et. al. 2007; Sedlák et. al. 2010). These have advanced the theories and methodologies of using land-cover data

and finely spaced weather sensors to monitor the effects of local geography on weather. They can generally be divided into two categories: long-term trials, where averages are of the greatest interest, or case studies with important but narrow research questions. Studies that contain elements of both, in an attempt to characterize their relative importance to the climate of a single location, are relatively rare.

One such study recently conducted in Trento, a city in the Italian Alps, found an average urban-heat-island [UHI] effect of about 3° C (Giovannini et. al. 2011). There, that figure varied considerably under different synoptic-scale regimes; in particular, the UHI weakened primarily due to cloud cover and resultant reduction in incoming shortwave radiation in the daytime, and due to wind speed and resultant increased mixing at night. The authors also concluded that the more complex the terrain in an area, the more local-scale processes dominate the climate. Other studies have focused on the role of vegetation height (Niachou et. al. 2008), building height (e.g. Georgakis and Santamouris 2006), drainage along slopes (Lookingbill and Urban 2003), or winds with upslope/downslope components (Sedlák et. al. 2010). The scales at which such effects occur span several orders of magnitude, from about 10 m to 10 km — the latter being smaller than the 13 km distance between gridpoints in the current highest-resolution operational model, the Rapid Refresh [RAP] model.

Such complexity greatly increases the challenge of forecasting on all timescales, especially because of the relative paucity of spatial data. Counting all sources, there are approximately 42,000 operational weather stations in the United States (Weather Underground). Excluding low-population Alaska, this amounts to one station per 193 km^2, or an average 7.8 km radius surrounding each station. Of course, stations are far from evenly distributed, and they are least likely to be situated where remote forecasts do the poorest job of estimating conditions: in regions of complex or varying terrain (Lookingbill and Urban 2003; Wang et. al. 2008). Various governmental agencies are in the process of laying the groundwork for the automated collection of personal-vehicle-based weather data, through programs like the Meteorological Assimilation Data Ingest System and the IntelliDriveSM initiative, but these face a number of regulatory and data-quality issues before they can be relied upon to greatly expand the network of available weather sensors (Mahoney et. al. 2010).

In the meantime, the existing network must serve as the source of all observation inputs and forecast verifications. Its imperfections mean that even National Weather Service [NWS] forecasts are often based more on *ad hoc* procedures and simple rules of thumb than on algorithms (Lahiff). For instance, in its forecasts for the Green and Adirondack Mountains, the Burlington, VT NWS office uses a blend of results from the Weather Research and Forecasting [WRF] model, the North American Mesoscale [NAM] model, and the Global Forecast System [GFS] model that are then combined with an empirically derived bias correction for each sub-region of the forecast area (Lahiff). However, neither there nor in this study area has there been an attempt to formalize these sorts of corrections, or to tailor them for particular microclimates or synoptic-scale regimes.

Overall, the literature review suggests that categorization and quantification of the net effect when all of the above-mentioned factors are simultaneously taken into account is a rare endeavor. This study aims to take on that challenge by analyzing elevation- and land-cover-influenced weather variations as an interlocking system, with the analysis

restricted to a few regions of interest at a few time periods of interest. That makes it more of a case study than a trial — but, in considering a range of factors that may influence local variations in temperature and moisture, the conclusions are sufficiently broad to be applicable in other areas with similar geographic complexity.

The original intent of the project was principally to investigate cold-air drainage on calm, clear nights, but the limited occurrence of such nights during the study period precluded that line of inquiry. In its place was developed a broader research question: what are the factors that influence the patterns of temperature change along elevation transects from night to night? The chief potential candidates supported by previous studies and theories are wind speed (e.g. Giovannini et. al. 2011), sky cover (e.g. Pypker et. al. 2007), and moisture (e.g. Lahiff). Geographic and topographic aspects of the transects themselves may also have a large role, especially in locations of typically weaker air movement, as cited above. And, finally, synoptic-scale atmospheric conditions and small-scale geographic features may combine to cause temperature differences between locations along a single transect (on the scale of the effects studied in Froelich and Schmid 2006 and Niachou et. al. 2008 among others) on the same night, in various proportions and under circumstances that this study aims to parse out.

Methodology

Three transects in the area immediately surrounding Ithaca, NY were selected for their large and relatively rapid elevation changes, and for their differences with respect to one other; they are numbered 1, 2, and 3 in the data and were intended to primarily represent land-water, field-forest, and rural-urban effects respectively (Figs. 1-4). Seven locally representative locations were chosen along Transects 1 and 3, while 12 were chosen along Transect 2 due to its greater length and diversity of surface features. These transect locations [TLs] were fixed throughout the course of the field campaign, which began on Nov. 4, 2013 and continued through Jan. 27, 2014. The TLs were numbered sequentially beginning from 1 for the bottom-most location and proceeding uphill. Using on-site measurements as well as online mapping tools like Google Earth, the transects were fully catalogued in terms of elevation, average and maximal slope in a 100-m radius of each TL, roughness length, nearby impediments to airflow such as vegetation and buildings, and distance to the nearest point on Cayuga Lake, the major local water body (using procedures and definitions from Linacre and Geerts 1999; Muller et. al. 2013; Sedlák et. al. 2010; and Wood et. al. 2013). Also developed and calculated for each location was an airflow convergence factor [CF] representing the strength of downslope drainage,

$$CF = \frac{h_u}{h_d} * \overline{m} \qquad [1],$$

where h_u is the percentage of the horizontal circle uphill from a point, h_d is the downhill analogue (with $h_u+h_d=1$), and $\overline{m}$ is the percent average slope of the surrounding area in a radius of ~100 m.

Six instruments were used: an Oregon Scientific THGR122NX hygro-thermometer, a Control Traceable 4392 hygro-thermometer, an Amprobe TH-1 hygro-

thermometer, a LaCrosse Technology WS-9023U-IT hygro-thermometer, a General 3MPE4 digital anemometer, and a Wind101 hand-held cup anemometer with vane and wind gauge that transmitted through a Sigma Sport BC 1609 logging display (Figs. 24-31). Select specifications for each instrument are included in its figure caption. These particular instruments represented the most-accurate devices on the market within the budget allotted to this study, with the redundancy intended to ensure the majority of the individual biases and imprecision could be identified and reduced, if not eliminated, in the final best-estimate reading.

Because this study primarily focused on nighttime airflow patterns, observations were taken in the evenings, at times ranging from just after sunset to 11 pm local time. A custom instrument housing with large openings to allow for rapid equilibration with surrounding conditions was attached to the rear of a personal vehicle and contained the first four instruments listed above, which were used to record all of the temperature and relative-humidity data at approximately the 2-m level (Fig. 32). Wind speed and direction were recorded at the same level using the two anemometers, both handheld. Data collection occurred at each location along two of the transects per evening, with transect pairings alternated to enable more-robust comparisons among all three. Equilibrium readings for most instruments were obtained upon arrival at the observation location (their quick adjustment being enabled by turbulent mixing resulting from 1-2 minutes' travel in the instrument housing at 50 $km*hr^{-1}$), and in the instances of steep temperature gradients where this was not the case a compensatory delay was made and noted.

Immediately before and after each observation-taking session, data were downloaded from six online sources: four that — in some cases via calculation — provided values that could be directly compared with the observed quantities, and two that provided information on synoptic conditions and lake-water temperatures. Among the former group are the RUC [Rapid Update Cycle] graphical forecasts for lower-atmospheric temperatures (at the 850 hPa, 900 hPa, 950 hPa, and 1000 hPa levels), where pressure-surface heights were calculated via the hydrostatic equation; gridpoint forecast soundings from the 13-km RUC model; observations from 12 regional private weather stations, publicly available on the website Weather Underground (www.wunderground.com); and official observations from the Ithaca weather station on Game Farm Rd [GFR]. A listing of the external stations, RAP/RUC gridpoints, and TLs, along with their metadata, is provided as Table 3, and a map as Fig. 4. All external data were temporally averaged, assuming linear change over the several-hour observation period. Two stations (DRYDE4 and DANBY1) were removed due to their missing data on 10 and 4, respectively, of the 18 observation nights. The other ten private stations and the public GFR station were used in computing regional-average temperatures and temperature changes against which local readings and derivative quantities could be compared.

From the data in quadruplicate generated by the four temperature and relative-humidity instruments, best-estimate values for temperature and dewpoint temperature were obtained by conducting an error analysis of the four primary instruments. Each was subjected to a rapid change in ambient temperature on the order of 20° C (i.e. by being moved from normal room temperature at 24° C to a refrigerator at 5° C) and its readings catalogued at 5-minute intervals until an equilibrium reading was achieved. By using

$$T_1 = T_0 - ((1 - 1/e) * (T_0 - T_{eq})) \qquad [2],$$

where T_0 is the initial value or the nth-degree threshold[1], T_1 is the $(n+1)$th-degree threshold, and T_{eq} is the externally verified equilibrium temperature, calculations were made to find the primary, secondary, and tertiary thresholds. This characterization of expected rates of temperature change is justified by the exponential prediction of Newton's Law of Cooling. By including the average number of minutes necessary to reach each threshold, time constants τ for each instrument i were obtained. Using these time constants, the instruments were then assigned weights, where the weighting for instrument 1 is given as follows:

$$W_1 = \frac{1}{\tau_1 \Big/ \sum_i \tau_i} \qquad [3]$$

Dividing the resulting weights by their collective sum yielded fractional weighting factors; each of these were then multiplied by the reading of their respective instrument to give the final, best-estimate result for each location, as used in all subsequent calculations and figures (Fig. 11).

Chauvenet's criterion was then applied to all instruments' temperature readings to test for outliers, which satisfy the equation

$$\frac{abs(x_i - \mu)}{\sigma} <= (D_{\max} * n) \qquad [4]$$

where x_i is the ith instrument's recording at a particular TL, μ and σ are the mean and standard deviations of the readings for that location, D_{max} is the z-score for the term on the left-hand side of the equation, and n is the number of instruments. Only four data points — one from the LaCrosse instrument on Jan. 26, the others from the Oregon Scientific instrument on Dec. 25 — needed to be removed, and the best-estimate results recalculated without them.

From the best-estimate observed temperatures T_O, adjusted temperatures T_A were calculated as

$$T_a = T_O + (loc - 1) * \frac{\Delta\overline{T}}{\Delta t} \Big/ 15 \qquad [5],$$

where $\frac{\Delta\overline{T}}{\Delta t}$ is the rate at which the regional-average temperature was changing during the 30 min-1 hour observation period, *loc* is the numerical assignment of the TL as described previously, and where it has been assumed that an average of 4 minutes elapsed between measurements at adjacent locations. This equation aims to, as nearly as possible, yield an instantaneous snapshot of conditions at the time when the measurement of the transect began. As a qualitative example, regionally falling temperatures would necessitate an upward adjustment of all subsequent measurements, with the correction increasing over time. The direction of travel along the transects varied, with the aim of eliminating bias introduced by poor linear time extrapolations in the uphill or downhill directions.

[1] Here, the threshold is the value that represents a percent decrease of 1-(1/e) from the initial value toward the equilibrium. Secondary and tertiary thresholds use the lower-degree threshold as the initial benchmark.

Though the dense spatial coverage and careful error analysis of this study makes its data reliable for the observation periods, temporally they constitute a narrow window. With the goal of generating predictor equations for the transects in mind, continuously transmitting instruments represent a good and indeed necessary source of raw data. Assuming the stationarity condition, development of a correlation between 'ground truth' and various nearby stations in the region would enable more-accurate forecasts for the TLs, at least on nights with similar conditions to the range of those encountered herein. To accomplish this, an extensive analysis was undertaken to determine the relative similarity of each TL to the suite of local weather stations. Comparisons between stations and TLs were made based on six variables: geometric distance, elevation difference, difference in distance to Cayuga Lake, difference in volume to Cayuga Lake[2], difference in local average percent slope, and difference in flow-convergence factor (Table 2).[3] As the middle two and last two essentially represent the same influences on conditions, two versions of the multidimensional analysis were executed for each transect on each night and compared with the observed values. The simpler version, consisting of a simple average of the geometric-distance, elevation-difference, and distance-to-lake-difference factors, was found to have the least error[4] over all dates and all transects (Fig. 12). It must be noted, though, that that figure also displays the "naïve error", i.e. from making a forecast for a TL simply by averaging the local-weather-station readings or RAP-gridpoint forecasts for the whole region; it performs barely, if at all, better than the best-version error, implying that as constructed the weighting factors play only a small role in improving the tailoring of forecasts to specific TLs.

These weighting factors were then employed to generate temperature predictions for each of the TLs, for the purposes of determining under what circumstances the greatest errors occur. A generalized form of the determining equation is

$$\sum_{i=1}^{12} WF_i * T_i \qquad [6],$$

evaluated for each TL, where WF_i is the weighting factor for a local weather station (see Table 3) and T_i is the temperature observed at that station. Additionally, such a procedure serves as a quality-control check on the study observations, especially for the first two dates when the instrumentation and procedures were still being fine-tuned. The same was done with the 13-km RAP forecasts, with TL forecasts being generated from the eight model gridpoints closest to the observation site (Fig. 4). As shown in Figs. 1-3, the

---

[2] Volume to lake is defined as the volume of air, in cubic meters, that lies between a location and the nearest point on the lakeshore. In calculating it, the slope between the location and the lake is assumed to be constant, so the volume of intervening air is found as ½*base*height, with b the geometric distance to the lake and h the difference in elevation. For the five locations at equal elevation as the lake, the volume was found as base*height, with h a mixing height of 17 meters (the depth of nighttime air flow observed in Sedlák et. al. 2010).

[3] Flow-convergence factor is the product of the local average slope and the ratio of the percent of the horizontal circle that is uphill from the location to that which is downhill. For instance, for an average slope of 5.0% and a percent uphill of 60% (i.e. a slight valley), the flow-convergence factor is 7.5.

[4] In the context of this paper, 'error' means the absolute value of T_F-T_O, where T_F is calculated with one of multiple approaches intended to approximate the observed value, which (despite the limitations of the direct observations, as discussed elsewhere) is taken to be the 'ground truth' at that particular position in space and time.

transects are 2-5 km in length, and the geometric distance between transects 1 and 2 is approximately 7 km; between transects 1 and 3, 5 km; and between transects 2 and 3, 9 km. This stands in contrast to the 13 local stations, only 5 of which are within 10 km of every TL. However, these latter were selected due to their sharing similar geographic characteristics with the TLs, such as those listed in Table 2.

Results

Throughout the results, particular attention is paid to Transect 2, it being the longest and most-diverse of the transects with respect to geographic features.

Referring to Figs. 5-7, normalized-temperature profiles were grouped into the following four quartiles based on their temperature lapse rate: $\Delta\theta/\Delta z > -2.8$ K/km (strong stability; Quartile 1), -6.9 K/km $< \Delta\theta/\Delta z < -2.8$ K/km (moderate stability; Quartile 2), -8.7 K/km $< \Delta\theta/\Delta z < -6.9$ K/km (weak stability; Quartile 3), and $\Delta\theta/\Delta z < -8.7$ K/km (neutral stability or instability; Quartile 4). The clustering of profiles within these groupings is particularly evident for Transect 2, where in Fig. 8 normalized temperatures at each TL are shown as differences from those at the bottom, color-coded by quartile. (Because the maximum elevation occurs at TL 10, the lapse rates were calculated as $T_{TL\ 10} - T_{TL\ 1}$.) Though by the above-mentioned definition the lapse rate on the night of Dec. 23 falls into Quartile 2 (teal line), visual inspection makes it clear that it is better considered as a member of Quartile 3, and subsequent analysis treats it as such. Similarly, Nov. 14 (thus labeled in Fig. 6) is better treated as an extreme than as an ordinary member of Quartile 4. Calculated mixing ratios are plotted on the same chart, colorized according to the lapse rate on the same night.

Upslope wind was calculated using a formula developed on the basis of the description in Sedlák et. al. 2010,

$$\begin{cases} -v\left(1-\dfrac{abs(D_{slope}-(D_{slope}-D_{wind}-90))}{90}\right), \text{ if } abs(D_{slope}-D_{wind})>180 \\ -v\left(1-\dfrac{abs(D_{slope}-D_{wind})}{90}\right), \text{ if } abs(D_{slope}-D_{wind})<180 \end{cases} \qquad [7],$$

where D_{slope} is the direction of maximal negative slope and D_{wind} and v are the wind direction and magnitude. It was found to be important in that study, where downslope cold-air drainage below tree canopies on steep hillsides was disrupted by above-canopy upslope winds if the latter was greater than about 2.15 m/s. The authors utilized a two-layer model substantiated by measurements at two different heights (Sedlák et. al. 2010). Though in this study all measurements were taken at the 2-m level, the concept of upslope winds was nonetheless considered useful, as the local-station data served as a source of average wind conditions untrammeled by the effects of nearby obstacles or slopes, which effects were prominent at most of the TLs. Measured lapse rates along the transects were of prime interest in this study, but they were not found to be significantly correlated with any of the variables save upslope wind[5]; one-sample t-tests of the means

[5] Upslope wind, in this usage, is that component of the average wind that is directed uphill along a slope oriented in a particular direction; for example, on the westward side of a hill, the upslope component would

of the upslope winds for each quartile, plotted in Fig. 9, showed that Quartiles 2 and 3 were significantly different from the overall mean, though in opposite directions, at the 5% and 0.1% levels respectively. This makes sense theoretically: in otherwise calm conditions, density differences dictate that upslope winds should be associated with weak lapse rates and inversions, and downslope winds with the strongest lapse rates, although increasingly strong wind speeds tend to dilute these effects via forced turbulent mixing.

Indeed, when there exists a gradient of a quantity, any movement of air acts to reduce that gradient by bringing air parcels with dissimilar values into contact. Further investigating the results through the prism of this concept, Figs. 17-20 show the along-slope gradients of potential temperature and mixing ratio, and the advection of relatively higher values of those quantities by the upslope/downslope component of the *locally observed* wind. The following sections examine the patterns within those figures one-by-one, aiming to parse out certain similarities that could hint at theoretical underpinnings of the phenomena, and that could be used in future to further refine forecasts.

The three nights with lapse rates exhibiting the most stability comprise Quartile 1 (Fig. 17). In all three there is a near-uniform increase of potential temperature with elevation, to which gradient the winds appear to be responding. Two important points are of note, though. First, this results in a downslope flow at the lower TLs (1-5), meaning that the effect of the along-slope temperature gradient itself dominates that of the temperature-induced vertical density gradient — overlying potentially warmer air flows downhill and acts to combat any potential inversion. Second, the clear signal of downslope flow at the lower TLs, where the slope is greatest, but not at the slopes above suggests the putative existence of a threshold of size or steepness necessary for a reservoir of air to contribute to such flows.

The strength of the lapse rates on these nights makes them the object of especial interest. In magnitude, they exhibit the three strongest and most-consistent-between-TLs downslope flows as well as the three steepest gradients of potential temperature. Advancing further with the idea of some kind of threshold or trigger, the magnitude of the smallest gradient of the three, observed on Dec. 4, is 1.3 K over an elevation difference of 150 m, for a vertical gradient of 8.7 K/km, close to the theoretical partially-moist-adiabatic lapse rate on that night of 7.1 K/km.[6] On the three nights in question, surface analyses from the NWS Weather Prediction Center Surface Analysis Archive (http://www.wpc.ncep.noaa.gov) revealed that each saw a high-pressure system situated several hundred kilometers to the north or northeast of the study site, resulting in south-to-southeast winds (Figs. 21-23). Combined with temperatures that were steady or rising, this implies a remnant inversion being entrained from above with potentially warmer air from an ultimately distant source, with a secondary local "source" on hilltops where greater prominence means more exposure to and influence by the regional mean flow.

For the middle quartiles (Figs. 18-19), two nights were fairly calm and two blustery from the west. However, they have in common very dry conditions at the top of the transect relative to the bottom. The dryness and the moderate lapse rates could both be attributable to a combination of strong winds and cloudy skies, which tend to increase

---

be 100% of the wind speed for a west wind, 50% of the wind speed for a northwest wind, and 0 for a north wind. Downslope wind is taken as the negative.

[6] Refer to the entry on the moist-adiabatic lapse rate in the American Meteorological Society Meteorology Glossary for equation used.

mixing and decrease differential cooling by radiation, respectively. The nights with neutral or unstable conditions (Fig. 20) similarly exhibited little coherence, as might be expected from their general lack of strong potential gradients in either temperature or moisture.

Figs. 10a and 10b show another observed correlation, that between along-transect lapse rates and regional temperature changes. When temperatures are rapidly falling, lapse rates tend to be greater (i.e. conditions tend to be more unstable), which would suggest a common cause for both phenomena — rapid radiative cooling eventually leading to the formation of inversions within a few hours of sunset. The tentative explanation behind this observation rests on the differential surface characteristics of the lower-most and upper-most TLs: especially for Transects 1 and 3, which commence in a shopping-plaza parking lot and adjacent to Cayuga Lake (Figs. 1 and 3), there is greater heat storage during the day, related to among other things the lower albedo and higher heat capacity of those areas. In the hours immediately following sunset, during which the bulk of the study was conducted, longwave radiation from those surfaces contributes to warmer temperatures at the bottom of the transects than otherwise. As discussed above, at a certain point when some parameter of the uphill cold-air reservoir is sufficiently large, downslope flow begins and builds an inversion by dawn. A worthy continuation of the project would be to examine conditions in the evening and predict, then verify, lapse rates before sunrise the following morning.

A fact seemingly at odds with this hypothesis is that there is no such universal relationship between along-transect lapse rates and percent cloud cover. Of course, cloud cover is not a perfect proxy; nonetheless, it prompts a more-nuanced view in which different factor may be at play. The pattern observed, wherein lapse rates cover a wide range of values under clear skies but cluster at middle values under greater cloud cover, leads to an alternative hypothesis that clouds play a distributional role in nighttime heat exchange, not merely a heat-trapping one. That is to say, with respect to effects on nighttime heat longwave re-radiation emanating from clouds seems to play a role opposite from that emanating from surface elements, the same conclusion reached in previous studies (Giovannini et. al. 2011; Pypker et. al. 2007). The greater the cloud temperature (for example, in the case of an approaching warm front), the greater the effect. Though in mid-latitude wintertime the presence of heavy cloud cover generally indicates the passage of a synoptic-scale cyclone and windy conditions, no other variables were found to correlate with along-transect lapse rates, including neither wind nor relative humidity.

Figs. 15 and 16 show the fruits of the effort made to generate forecasts for the TLs of Transect 2 from two sets of external data. The first comes from local weather stations, the second from nearby RAP-model gridpoints (Fig. 4; Table 2). The absolute forecast errors $T_{forecast}$-T_{obs} are shown, pooled by observed lapse rate as a proxy for the varying conditions under which the forecasts have been tested. The results indicate a close match between the two empirical forecast methods — they are much more similar to each other, in fact, than to the observed values on the ground, suggesting that the dominant effects driving inter- and intra-transect differences cannot be well approximated using data from elsewhere in the region.

This is an especially interesting result because, in addition to data-quality issues for the local stations and resolution issues for the RAP model, deriving forecasts from the

two fundamentally involves comparing parametrized forecasts for points in isolation and observations that reflect processes occurring in the surrounding complex region. To have them be almost indistinguishable is a strong vote of confidence for the fidelity of the model. Errors increasing from bottom to top may simply be a consequence of the predominance of lower-elevation stations and gridpoints in these analyses — inevitable, since TLs 9-12 of Transect 2 are among the highest points in the region. The only overestimation of temperatures at bottom locations occurs when conditions are unstable, despite the advection of potentially warmer air from upslope, at least for Transect 2 (Fig. 17). Also, notwithstanding the at-length discussion of the role of mixing in affecting conditions on the nights observed, the forecasts' underestimation of temperatures near the bottom of Transect 2 and overestimation near the top independent of lapse rate suggest an inherent inability to capture the role of some key variable, with wind being a prime candidate.

As a final piece of analysis, the linear-regression equations linking observed along-slope lapse rates with region-wide temperature changes, upslope-wind strength, and modeled open-sky lapse rates were combined with the observations at the bottom of the transect to predict those at the top. The average absolute errors from this procedure are plotted in Fig. 14. This result leaves the experimental-forecast section on a hopeful note, because all three of the variables can be determined (or at least well-estimated) without needing to be on-site, thus suggesting the possibility that with further calibration such a scheme could be used to accurately make predictions for each TL, or for transects elsewhere.

Conclusions

Though much more work could be devoted to the topic, some conclusions can be drawn from the results at hand. As in a number of previous papers, in particular Sedlák et. al. 2010 and Giovannini et. al. 2011, winds appear strongly associated with differential weather conditions along slopes. Whether such correlations represent causation, reverse causation, or mere correlation is in many cases still unclear, although it is certain that these winds are acting to reduce gradients in all quantities for which one exists, in this study temperature and moisture being principally of interest. Comparing lapse-rate quartiles resulted in few categorical differences, although neutral and unstable lapse rates show the most promise in terms of having distinct characteristics of local- and synoptic-scale conditions. The idea of downslope drainage as a trigger emptying a reservoir, or similarly of a plateau with a minimum requisite slope, was not found in a review of previous literature but appears to have promise and bears future interest. The forecast mechanisms performed reasonably well despite their many imperfections, and the broad correlations identified, if implemented or corrected for, should improve their performance in the types of terrain studied here. The improvement in skill shown by the three-factor forecast scheme lends credence to the idea that the factors included are indeed important ones, and that further work to enable generalization would be both possible and productive.

Potential Errors

As with all studies that are observational in nature, and whose methodology and instrumentation must be specially developed, there were a number of ways in which error may have been — and in some cases, very likely was — introduced, as discussed below.

a. One simple error comes directly from the instrumentation. Multiple instruments were used to attempt to minimize this problem, and they were inter-correlated as they moved in and out of rotation during the first few weeks, but as the corrective weighting factors were based on a fairly small sample size of trials, they may well have been inaccurate in some way.

b. Differing response times meant that the 'slowest' thermometers accrued error if the temperature changed rapidly along the transect. This issue was addressed by waiting until the majority had reached approximate equilibrium, and noting the discrepancy – complete equilibrium is impossible if (as is the case) external temperatures are continuously varying.

c. All measurements were taken alongside road right-of-ways, and therefore comprise an internally consistent group of data, but if conditions near roadways are significantly different than those elsewhere in the local area (e.g. due to the gap in trees and buildings, or the lower albedo of the pavement) then these measurements do not best represent the local climate as a system. Similar problems may have been generated from the influence of the vehicle on both temperature and moisture readings.

d. Simple reading or transcription error may also have been introduced.

e. For wind readings, 30-sec or 1-min averages were taken and assumed to be a representative sample of the wind at that location throughout the transect measurement period. Also, rounding of directions and speeds created uncertainty.

f. Similarly, transect measurement periods were not of negligible length, but varied from 30 min to 1 hour. This was counter-acted by introducing an 'adjustment' at each location based on region-wide average parameter changes during that time period and an average of 5 min per location, but any errors in those figures, or in the applicability of the figures to the specific evening and transect in question, would produce temperatures not indicative of a true transect 'snapshot'.

g. Because station characteristics such as slope, % uphill, and elevation were hand-measured or obtained from maps of various kinds, there is a certain amount of uncertainty inherent in them.

h. Regional observations (at official and unofficial weather stations) were recorded for two time points, one before and one after each set of transect measurements, with values in between being calculated by assuming linear change over that several-hour period. Non-linear change would mean that an error of up to several tenths of a degree C was introduced in the proper readings of those stations.

i. Private local weather stations have their own sets of uncertainties, biases, and one-time errors that are for the most part difficult to detect in small sample sizes. Thus, data from these sources have been considered less trustworthy than self-collected data, or data from official stations such as that at Game Farm Rd.

j. RUC forecast temperatures were approximated from values plotted on a map and thus have maximum uncertainties of approximately +/- 0.25° C.

k. Forecast soundings are for the RAP gridpoint in Lansing (about 10 km north of Ithaca), so this also introduces uncertainties of a similar magnitude.

Future Work

Multiple sophistications could be made in terms of methodology, instrumentation, and location to obtain a different, larger, and perhaps more-generalizable dataset. Expanding the size of the dataset to enable more statistically significant conclusions is of primary importance, preferably in the same locations. Doing so in a manner that would better test the predictive power of forecasts, whether modified by weighting factors or not, would in some ways be the ultimate test. Selecting different sites with similar characteristics would also provide a good measure of the universality of some of the conclusions reached herein. Obtaining observations at two levels, perhaps at the 1-m, 2-m, and 4-m levels as in Sedlák et. al. 2010, would help separate out the scales on which temperature, moisture, and wind interact.

A particularly notable result is the correlation between "slope" lapse rates, as measured along the transects, and "sky" lapse rates, as calculated by taking the difference of the RAP-model temperature predictions at 1000 hPa and 950 hPa. Rather than a one-to-one relationship, as might be expected, the measured slope lapse rates were generally ¾ of the sky lapse rates. The question of whether this is an artifact of the model inaccurately representing boundary-layer processes that tend to cool the surface at night relative to the atmosphere, of representing them correctly but at different heights (assessed via comparison to observations at the equivalent elevations for each night), or of perhaps poorly resolving some site-specific factor like a surface geographic feature, must be left for future investigation.

Figures and Tables

1. Transect 1: A 110-meter rise in elevation over 2.3 km, with elevation increasing from southwest to northeast. Primarily serves to determine the effect of the lake on nightly cooling at different distances and elevations.

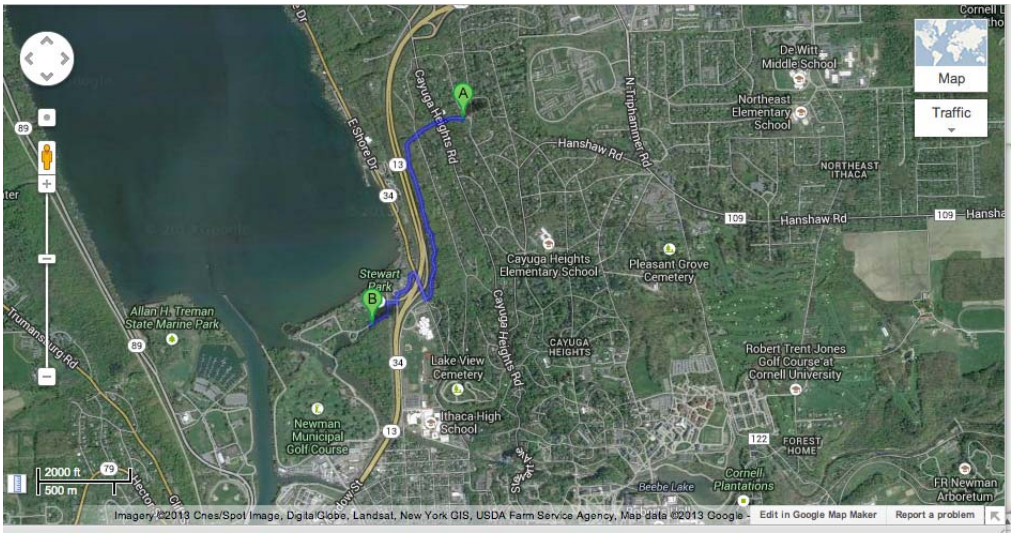

2. Transect 2: A 250-meter rise in elevation over 5.2 km, with elevation increasing from west to east. Primarily serves to determine the effect of fields and forests.

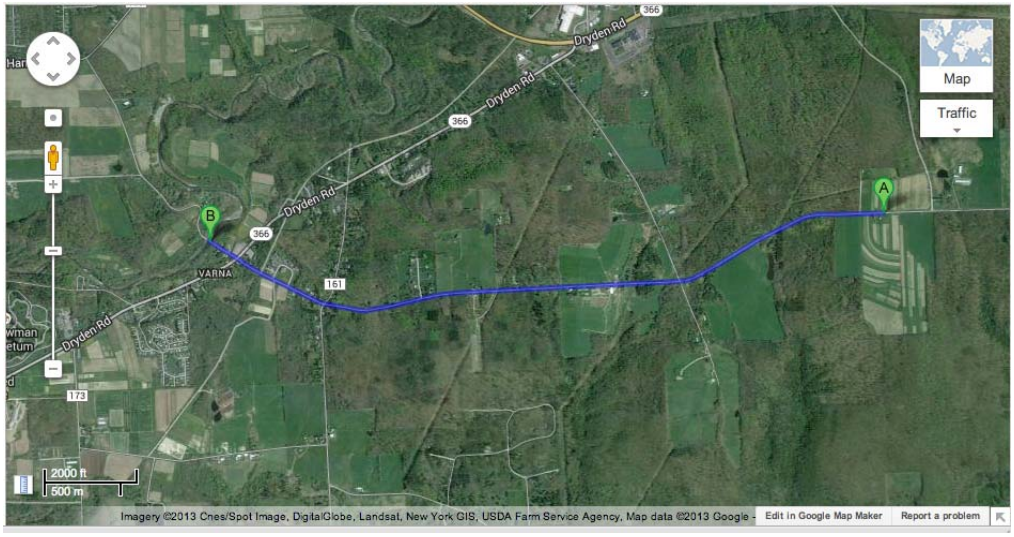

3. Transect 3: A 175-meter rise in elevation over 2.6 km, with elevation increasing from north to south. Primarily serves to determine the effects of urban vs. rural land-cover types.

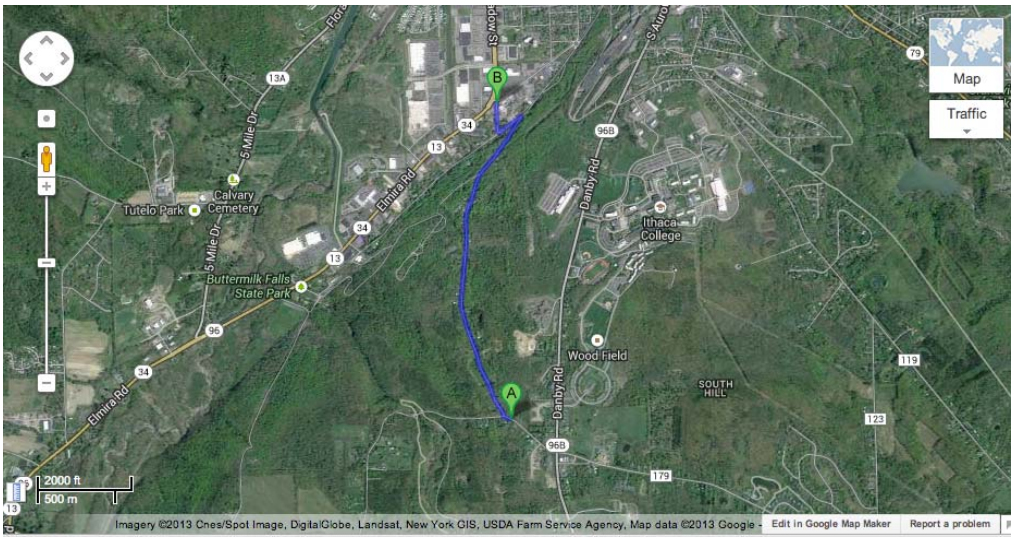

4. The transects, plotted in blue and numbered clockwise from the north, in the context of the externally sourced observations of various types: Weather Underground local stations are in pink, the Game Farm Rd. official station is in green, and RAP gridpoints are in yellow. The forecast soundings used were for the Lansing RAP gridpoint (the second-most northerly one with a dark shadow in this rendering).

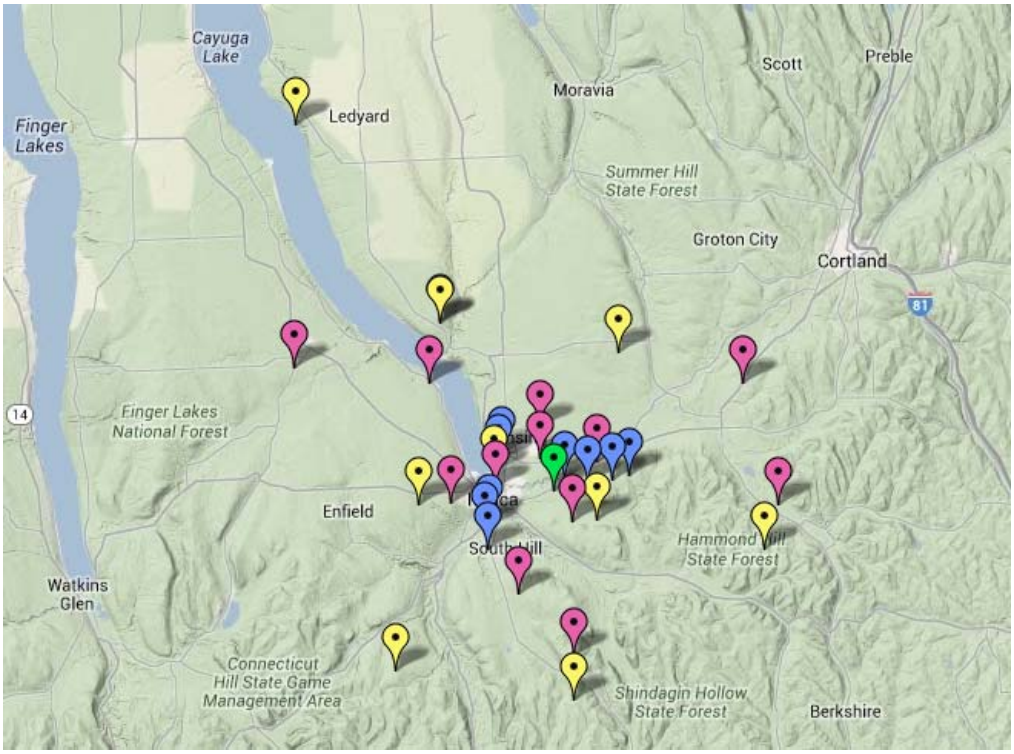

5. Thirteen nightly temperature profiles for Transect 1, shown as differences in potential temperature from the value at the bottom location, with elevation increasing to the right.

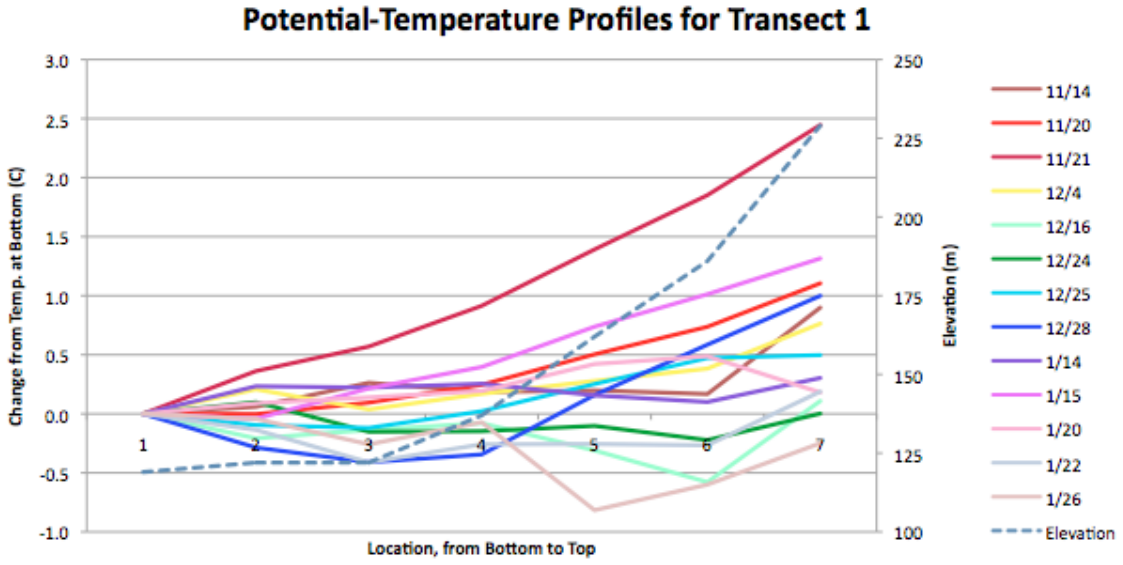

6. Twelve nightly temperature profiles for Transect 2, with the same format and temperature scale as above.

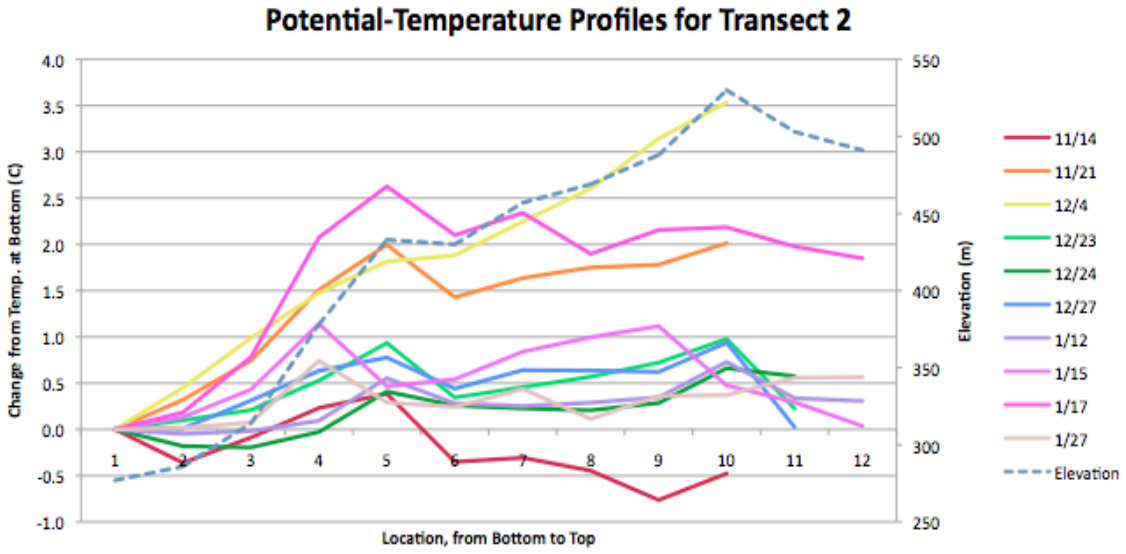

7. Eleven nightly temperature profiles for Transect 3, with the same format and temperature scale as above.

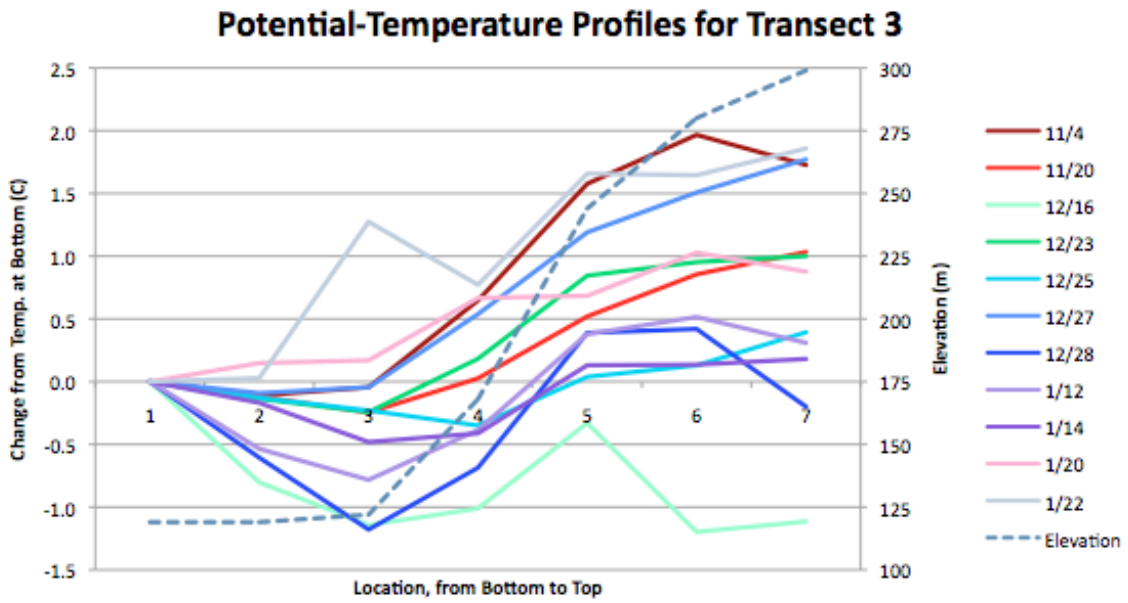

8. Normalized temperatures (solid lines; left axis) and mixing ratios (dashed lines; right axis) at each transect location, with colors indicating the four quartiles as defined by the lapse rate and described in the text.

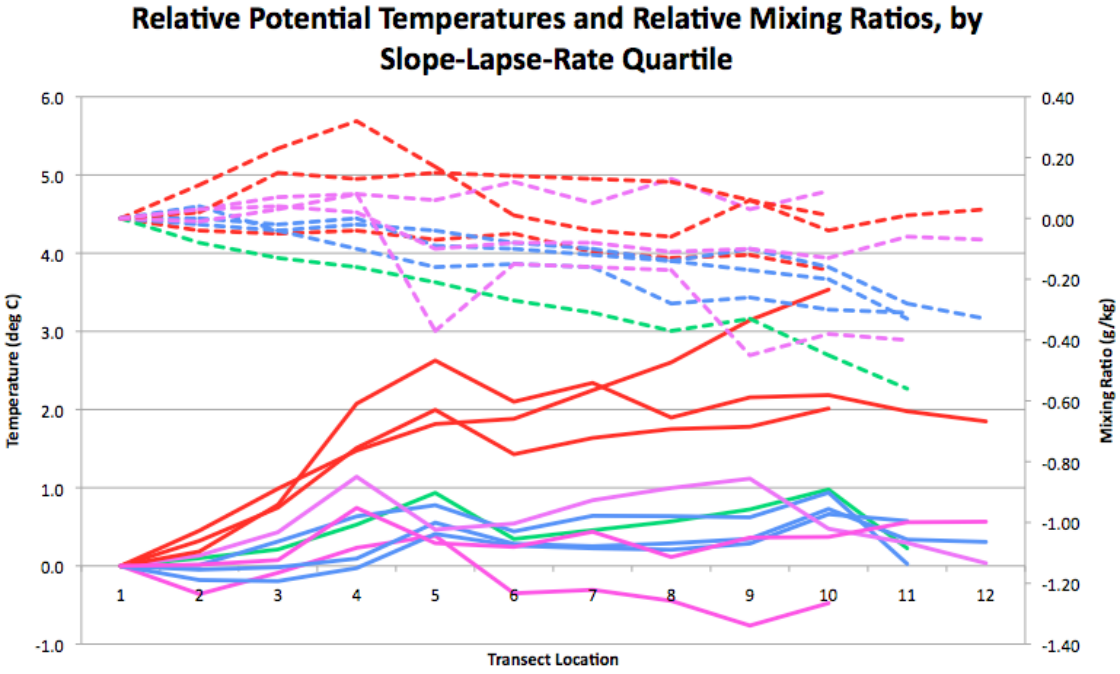

9. A correlation scatterplot showing the pattern in the calculated upslope component of regional winds, when grouped by lapse-rate quartile. The MALR on most nights was between 6.0 and 7.0 K/km (here, the divide between Q2 and Q3 is at 6.9 K/km).

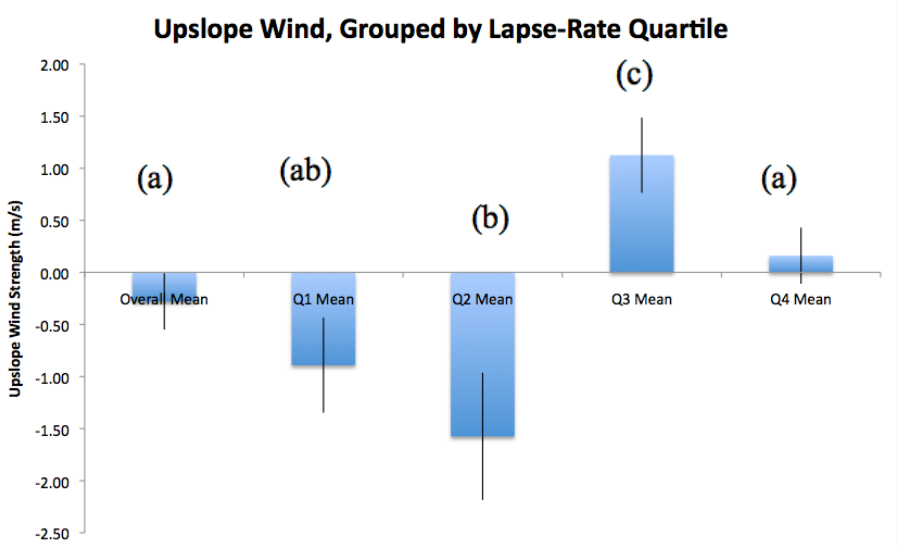

10a and 10b. Correlation scatterplots between mean region-wide temperature changes and lapse rates for all three transects, separated according to the observed sky cover. Rapidly cooling regional temperatures are associated with higher lapse rates — as the hills cool more quickly — and steady or rising temperatures are associated with inversions — possibly due to entrainment from above — but only under clear skies.

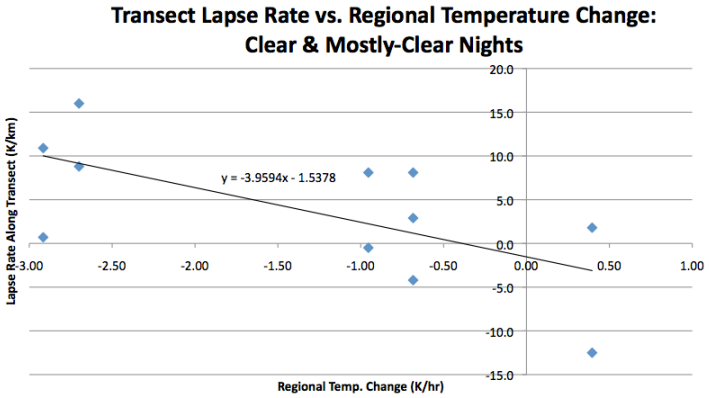

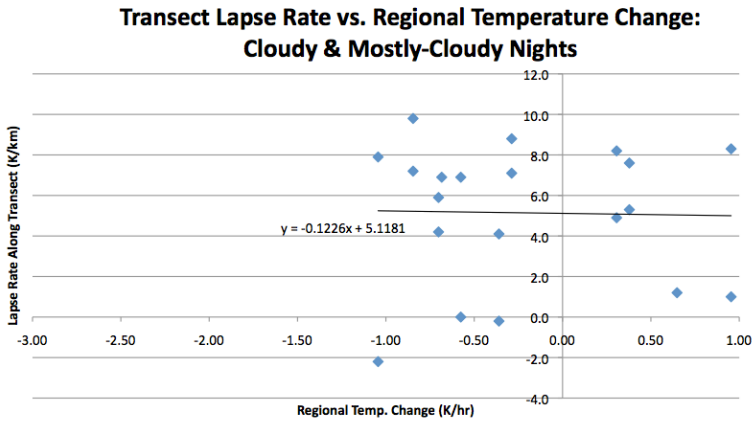

11. A chart showing the temperature measurements recorded on five of the instruments on a sample night, the best-estimate values calculated based on the relative time constants, and the adjusted-best-estimate values taking into account the *increase* in regional temperature that occurred during the hour-long observation period.

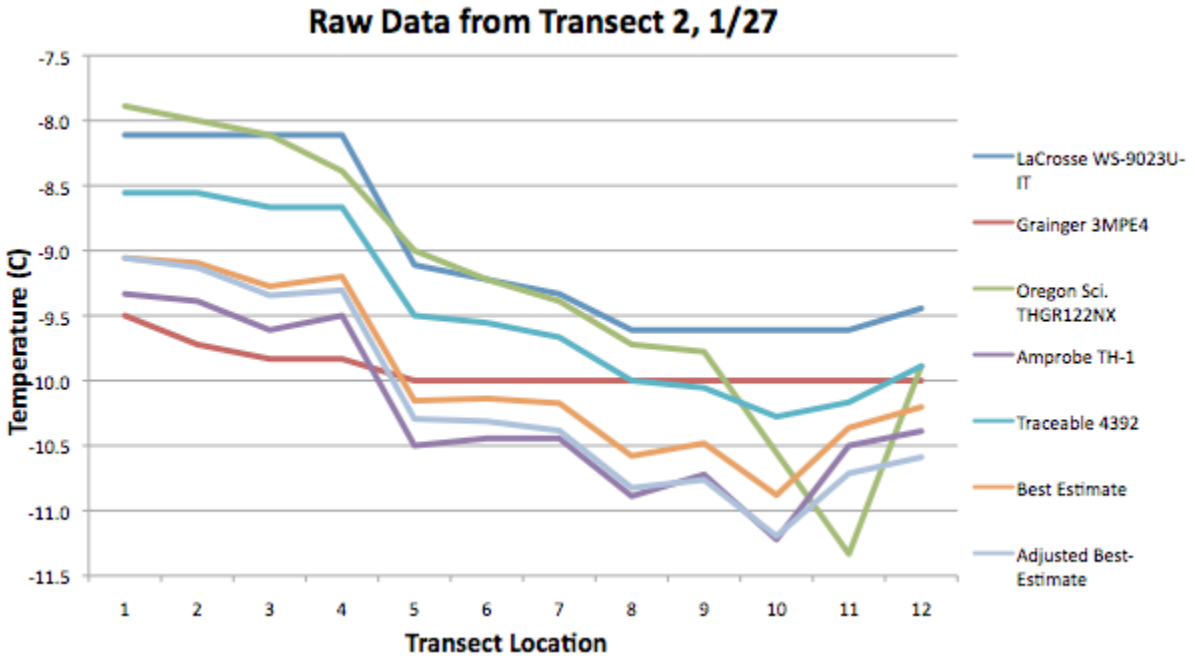

12. On this chart, the height of each bar represents the error (averaged over all locations and nights) resulting from making best-estimate forecasts using three different weighting schemes. Error bars represent standard errors. In Version 1, the bases of comparison are geometric distance, elevation, and distance to the nearest point on Cayuga Lake; in Version 2, elevation, volume to lake, and airflow convergence factor; and in the Naïve version, no weighting is done whatsoever (i.e. the forecast for each TL is identical and is a simple average of all the local stations or RAP gridpoints, respectively).

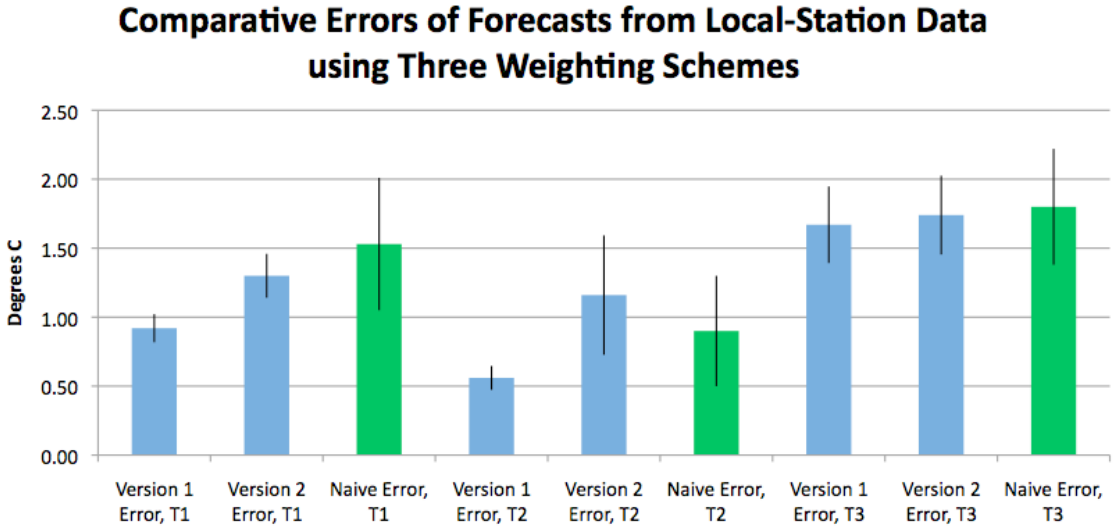

13. Same as Fig. 12 but for forecasts generated from RAP-gridpoint data instead of from local stations.

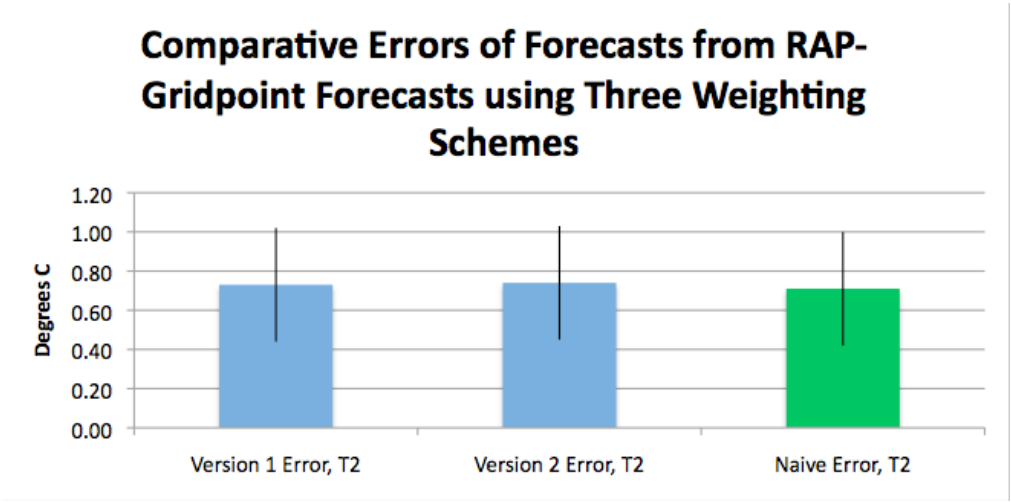

14. Comparative errors of the best-estimate Version 1 forecasts, their naïve counterparts, and the three-factor forecast that combines regressions of upslope-wind strength, the modeled open-sky lapse rate, and the region-wide temperature change.

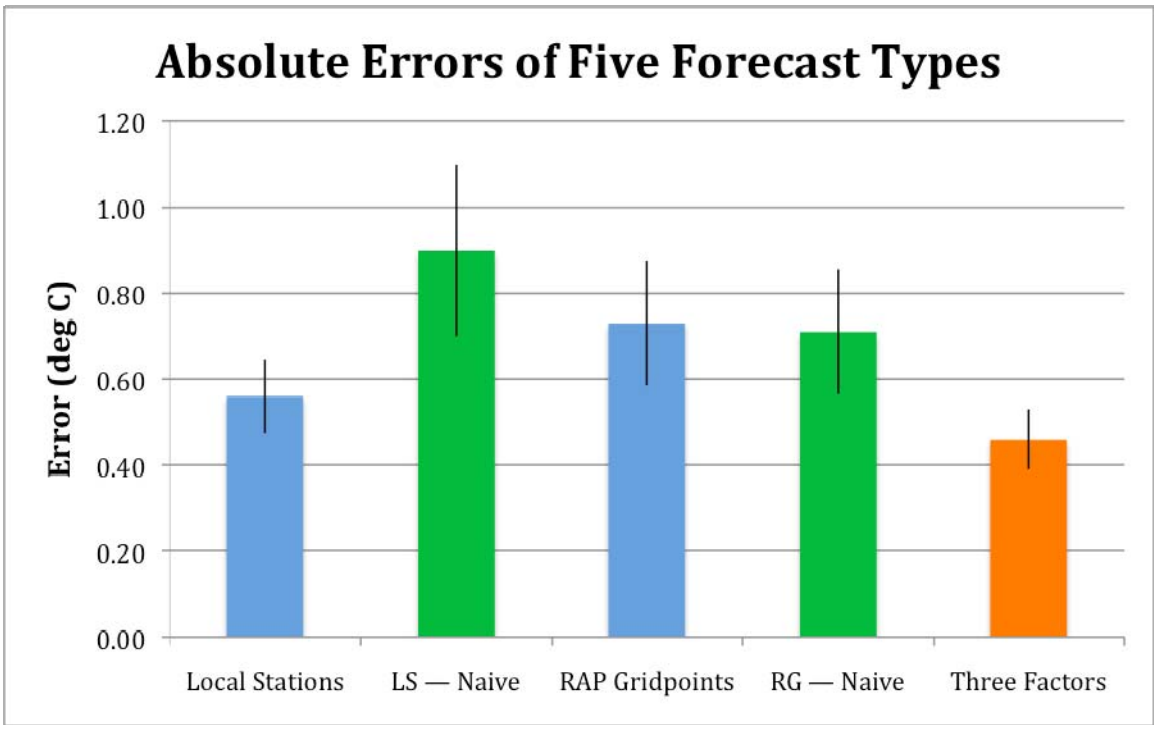

15. Plotted on this chart are average errors for Transect 2 obtained with the best-estimate local-station-derived forecasts. The nights were grouped into transect-specific quartiles based on their observed lapse rates relative to the set of lapse rates along that transect. Lines are averages from among the nights in that grouping, with shaded areas representing the spread (due to the small sample size, only one night fell into the 2nd quartile, which may be treated as part of the 3rd quartile; see discussion).

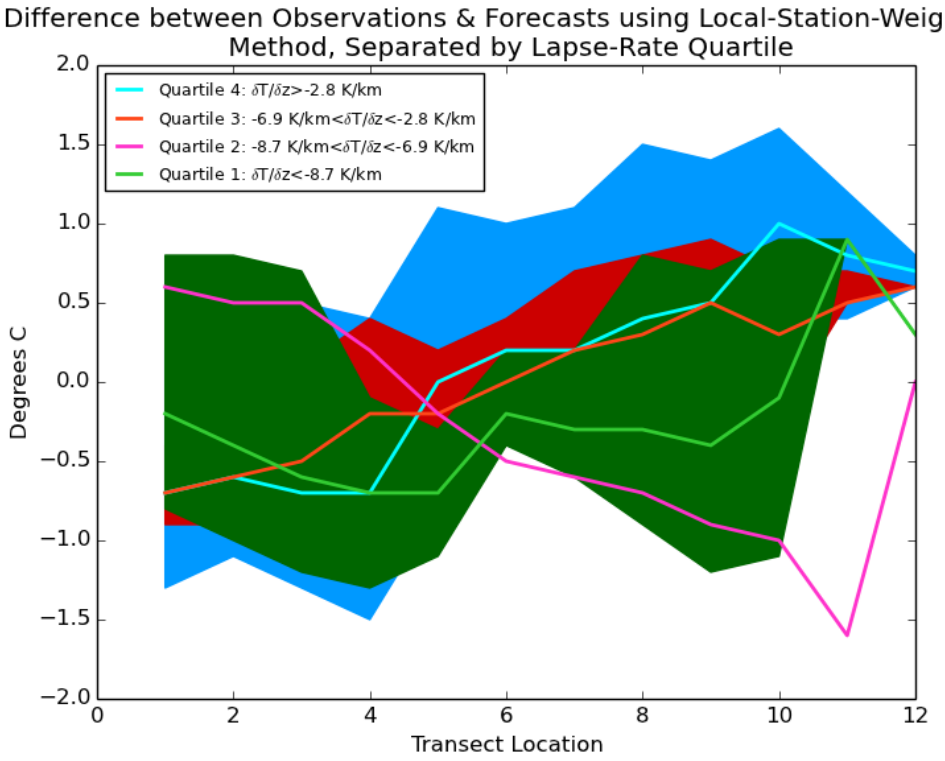

16. Same as Fig. 14 but for forecasts made using RAP-gridpoint forecasts rather than local-station observations.

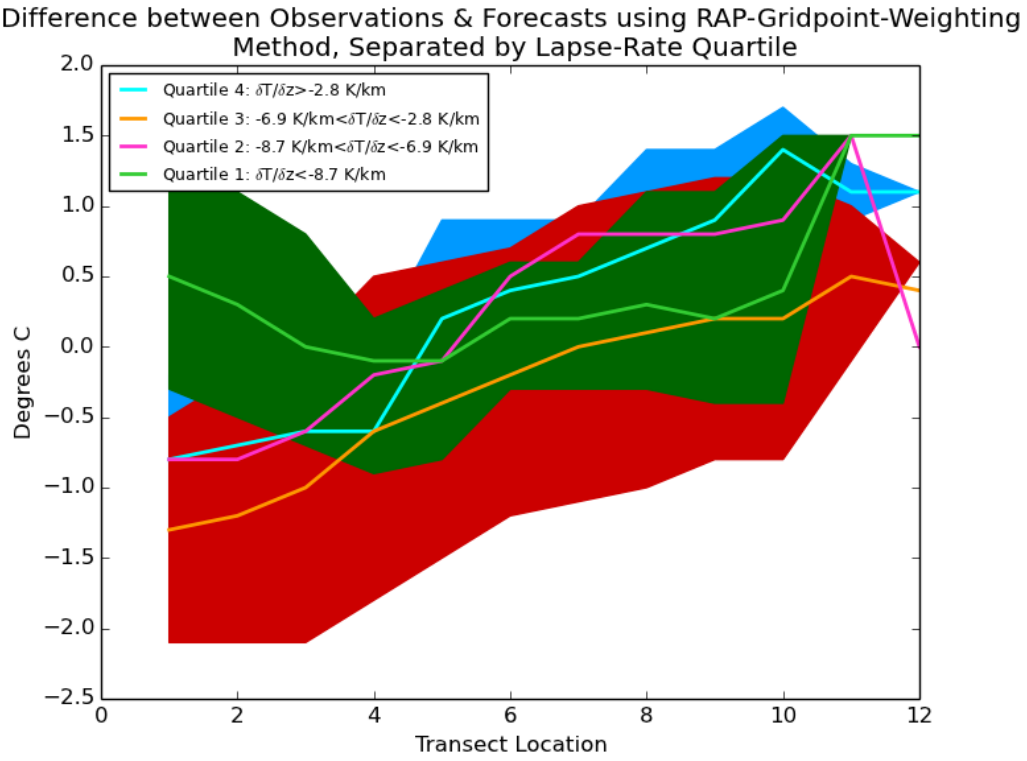

17. For nights on Transect 2 when the observed lapse rate $\Delta T/\Delta z > 8.7$ K/km (Quartile 1), potential temperature θ and mixing ratio ζ are plotted as differences from the value at the bottom of the transect. Text is shown in blue if the calm-air flux for that quantity is to the left at that location (generally downslope); red if to the right (upslope); purple if convergent; and black if divergent. Arrows represent the upslope/downslope component of the measured winds at each location, i.e. the approximate type and strength of advection.

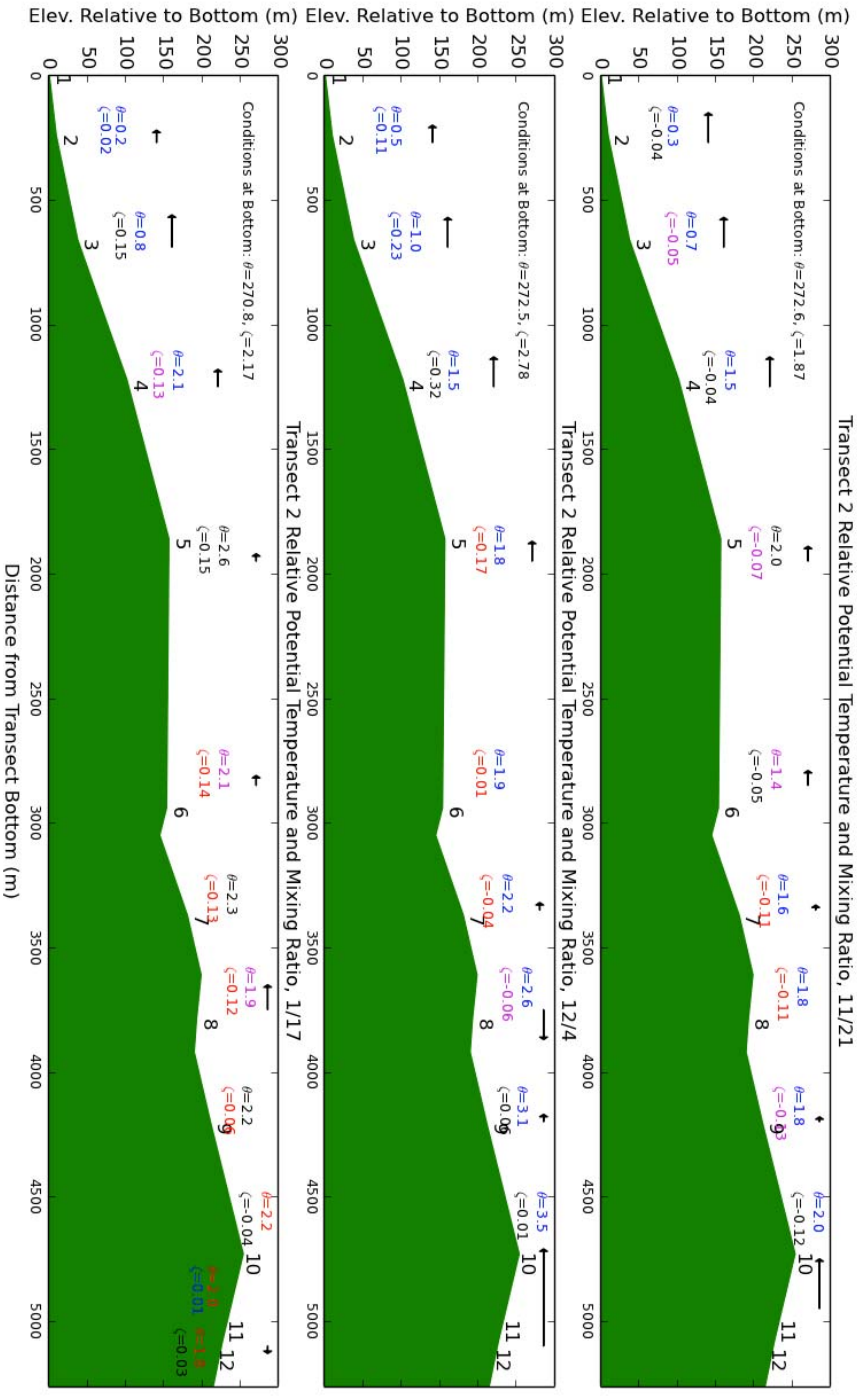

18. Same as Fig. 17 but for nights with observed lapse rates 8.7 K/km > $\Delta T/\Delta z$ > 6.9 K/km (Quartile 2).

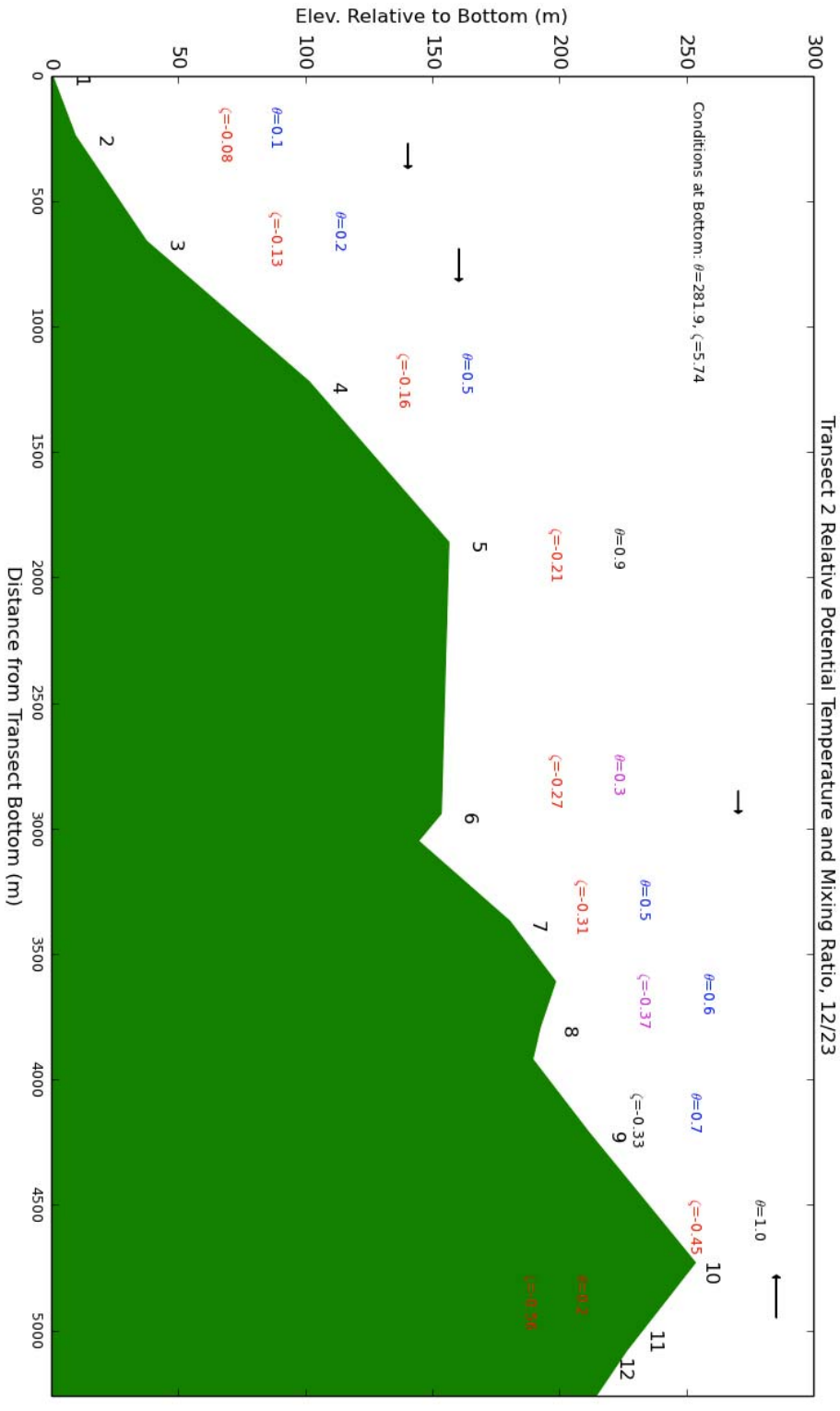

19. Same as Fig. 18 but for nights with observed lapse rates 6.9 K/km > ΔT/Δz > 2.8 K/km (Quartile 3).

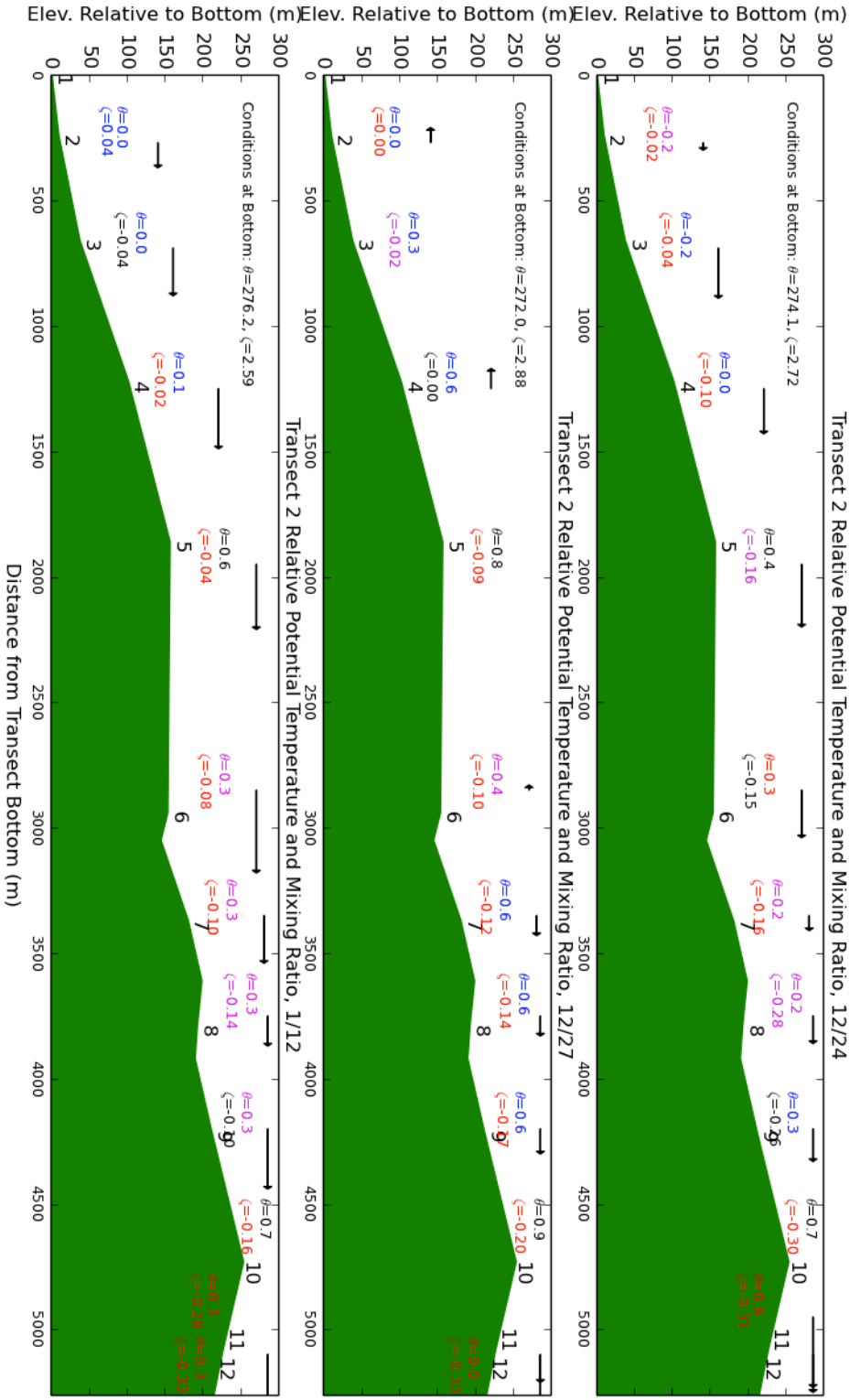

20. Same as Fig. 19 but for nights with observed lapse rates $\Delta T/\Delta z < 2.8$ K/km (Quartile 4).

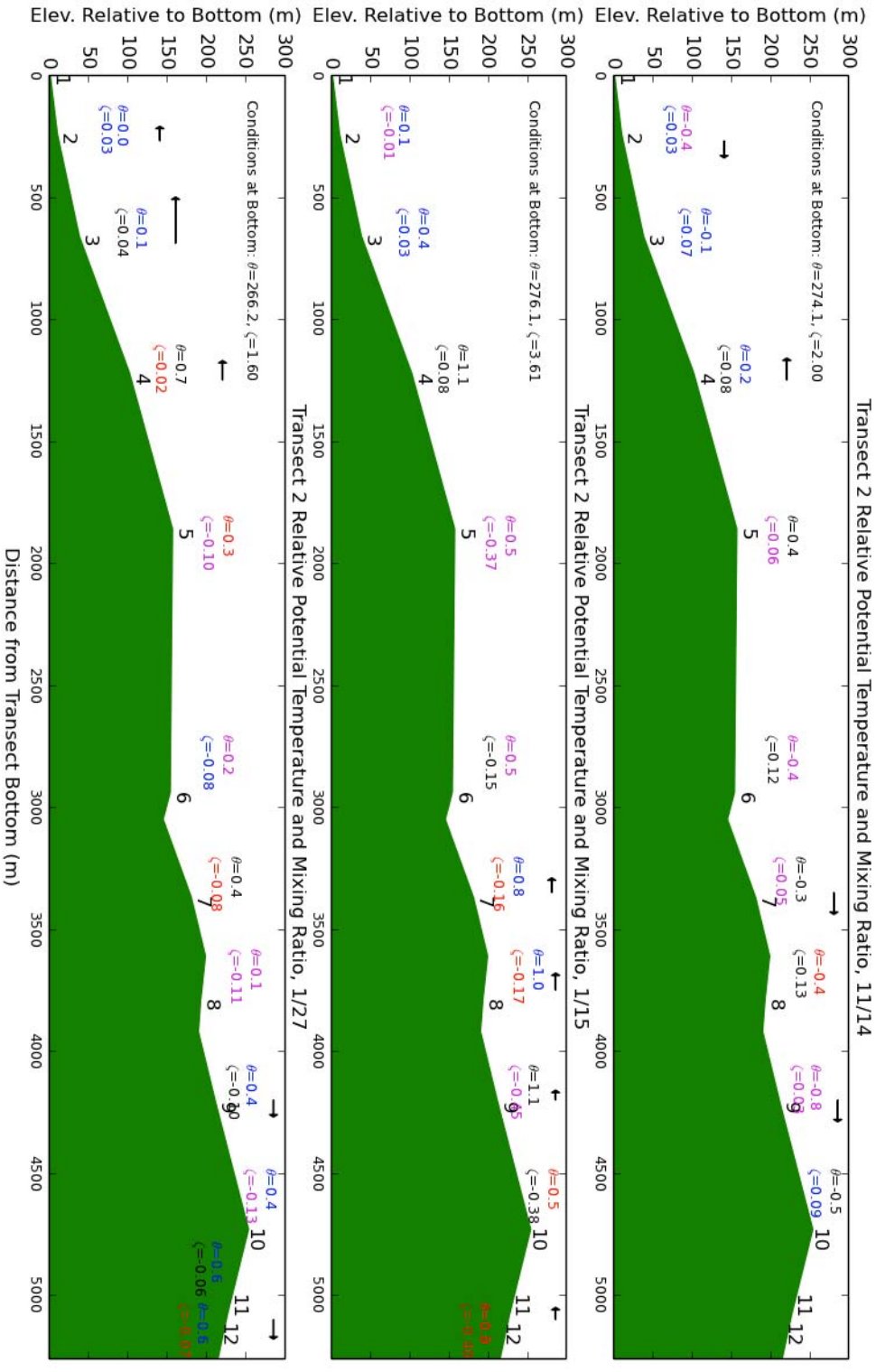

21. Synoptic conditions on Nov. 21, 2013, at 03Z.

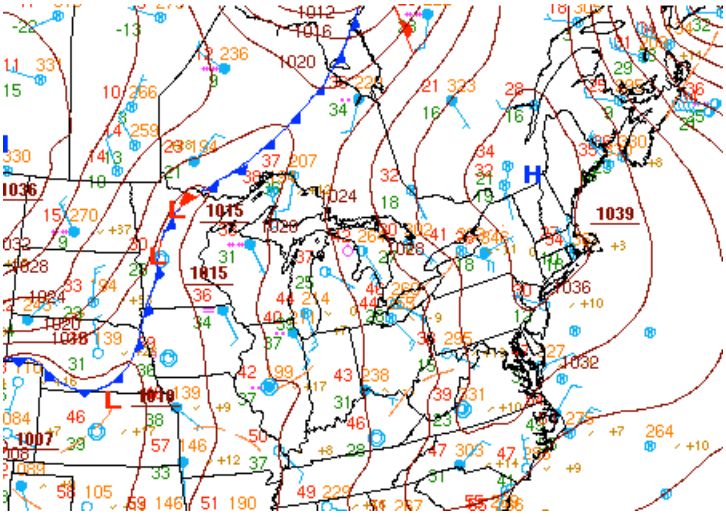

22. Synoptic conditions on Dec. 4, 2013, at 03Z.

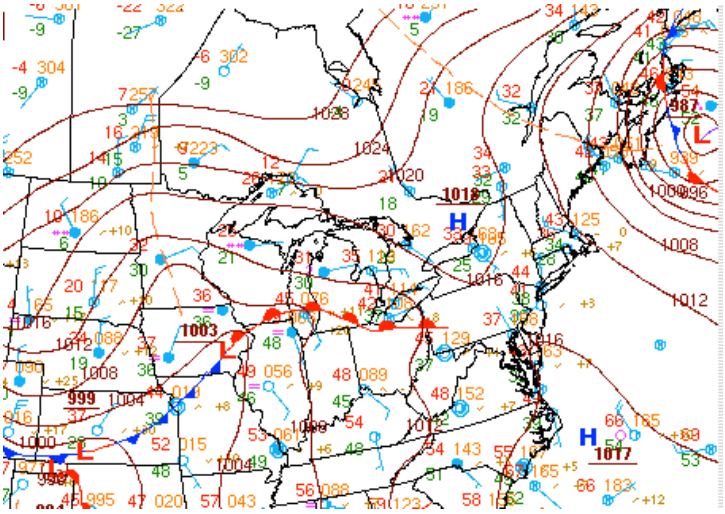

23. Synoptic conditions on Jan. 17, 2014, at 03Z.

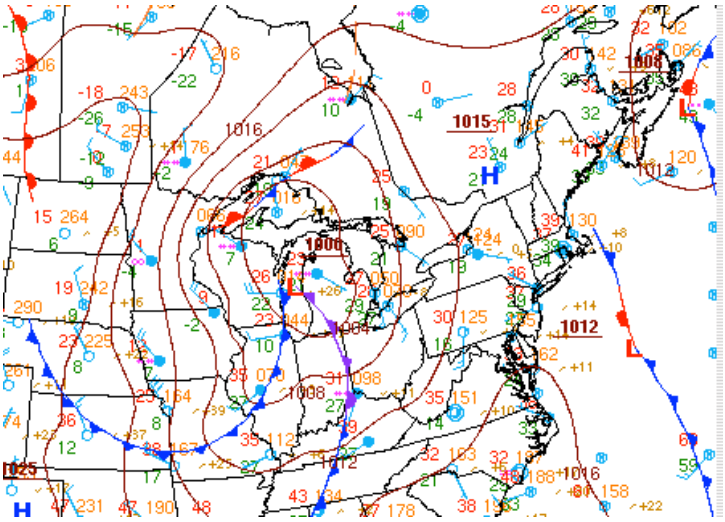

24. Oregon Scientific THGR122NX hygro-thermometer. Accuracy: 0.3° C. Response time: 40 sec. Time constant: 7 min. RH accuracy: 3%.

25. Control Traceable 4392 hygro-thermometer. Accuracy: 0.5° C. Response time: 1 sec. Time constant: 1.5 min. RH accuracy: 3%.

26. Amprobe TH-1 hygro-thermometer. Accuracy: 0.4° C. Response time: 10 sec. Time constant: 1 min. RH accuracy: 4%.

27. LaCrosse WS-9023U-IT hygro-thermometer. Accuracy: 0.9° C. Response time: 15 sec. Time constant: 3 min. RH accuracy: 4%.

28. LaCrosse WS-9023U-IT sensor, inside of the instrument housing.

29. General 3MPE4 digital anemometer. Accuracy: 0.1 mph. Minimum wind speed: 1.2 mph.

30. Wind101 cup anemometer with wind vane. Minimum wind speed: 0.5 mph.

31. Sigma Sport BC 1609 logging display. Accuracy: 0.1 mph. Minimum wind speed: 1.0 mph. (Temperature function not used.)

32. The instrument housing as it appeared during the observation period (though with the LaCrosse display resting on top located inside the vehicle). Each of the previous thermo-hygrometers were securely attached at various places inside the housing such that the airflow past them was as unimpeded as possible, and that their displays were easily visible without having to take apart the contraption.

Table 1. A sample data table showing the best-estimate observations of the various quantities, some of the transect metadata, and the comparison data from local weather stations.

Transect 2	*1/27, ~0000 Z*	Cloudy, light snow

Consolidated Data

Location	Temp. (C)	Adjusted Temp.	Dewpt. Temp. (C)	Wind Speed (m/s)	Wind Direction	Elev. (m)	Dist. to Lake (km)	Rel. Hum. (%)
1	-9.1	-9.1	-13.3	1.0	113	277	5.2	81.1
2	-9.1	-9.1	-13.0	1.8	158	286	5.4	82.5
3	-9.3	-9.3	-12.8	3.6	135	314	5.8	84.2
4	-9.2	-9.3	-13.0	0.7	90	377	6.3	83.4
5	-10.2	-10.3	-14.2	1.6	180	432	6.8	82.5
6	-10.1	-10.3	-13.7	6.8	180	429	7.9	84.3
7	-10.2	-10.4	-13.8	2.7	180	457	8.4	84.2
8	-10.6	-10.8	-13.9	8.1	180	469	8.7	85.9
9	-10.5	-10.8	-13.9	2.3	203	487	9.1	85.6
10	-10.8	-11.2	-14.0	9.0	180	530	9.6	86.8
11	-10.4	-10.7	-13.5	5.9	180	502	9.9	86.9
12	-10.2	-10.6	-13.5	2.7	203	490	10.1	86.5
G.F. Rainwise	-8.9		-13.4	4.5	135	293	5.2	70.0
KNYTRUMA2	-8.3		-11.1	2.3	180	309	6.0	80.4
KNYITHAC15	-7.6		-11.7	1.1	180	166	0.2	72.6
KNYITHAC7	-9.3		-12.2	5.4	180	354	3.5	79.0
KNYITHAC1	-7.0		-13.1	1.4	135	119	1.5	62.2
KNYITHAC14	-9.3		-12.2	4.1	158	358	8.0	79.0
KNYITHAC12	-9.3		-12.2	0.0		335	9.0	79.0
KNYITHAC16	-8.9		-16.7	0.5	135	313	4.0	53.3
KITH	-8.7		-17.8	0.0		313	4.5	
KNYDRYDE3	-10.0		-13.9	8.1	158	441	19.0	73.2
KNYDRYDE4	-17.8		-17.8	0.0		372	21.0	
KNYDANBY1	-10.9		-13.1	3.2	180	513	14.5	84.3
KNYITHAC17	-9.8		-12.8	2.3	158	435	9.5	79.0
RUC 1000 hPa	-7.8					58		
RUC 950 hPa	-10.0					454		
RUC 900 hPa	-12.5					868		
RUC 850 hPa	-13.8					1303		

Table 2. A listing of all the stations and transect locations used in this study, along with their most important metadata.

Station/Location	Elev. (m)	Dist. to Lake (km)	Vol. to Lake (m^3)	Local Avg. Slope (%)	Conv. Factor	Lat. N	Lon. W	Sfc. Rough-ness	Sky-view Factor (%)
Game Farm Rd.	293	5.2	-77201	0.0	0.0	42.45	76.45		
KNYTRUMA2	309	6.0	-74024	2.3	3.5	42.53	76.68		
KNYITHAC15	166	0.2	-6826	6.7	6.7	42.52	76.56		
KNYITHAC7	354	3.5	-19438	4.2	2.8	42.44	76.54		
KNYITHAC1	119	1.5	22866	0.0	0.0	42.45	76.50		
KNYITHAC14	358	8.0	-38854	9.5	9.5	42.43	76.43		
KNYITHAC12	335	9.0	-75491	14.5	14.5	42.47	76.41		
KNYITHAC16	313	4.0	-46933	4.0	4.0	42.47	76.46		
KITH	313	4.5	-52800	1.8	1.8	42.49	76.46		
KNYDRYDE3	441	19.0	147845	11.3	11.3	42.52	76.28		
KNYDRYDE4	372	21.0	-58083	1.8	1.8	42.44	76.25		
KNYDANBY1	513	14.5	271827	7.0	7.0	42.34	76.43		
KNYITHAC17	435	9.5	65095	6.7	6.7	42.38	76.48		
RAP Lansing	232	1.5	-36691	n/a	n/a	42.56	76.55		
RAP Enfield	384	4.4	-3947	n/a	n/a	42.44	76.57		
RAP Danby	463	17.7	197877	n/a	n/a	42.31	76.43		
RAP W. Dryden	399	11.1	15730	n/a	n/a	42.54	76.39		
RAP Ellis Hollow	366	8.4	-30928	n/a	n/a	42.43	76.41		
RAP Aurora	119	0.0	0	n/a	n/a	42.69	76.68		
RAP Harford	573	20.9	583947	n/a	n/a	42.41	76.26		
RAP Newfield	500	16.1	269655	n/a	n/a	42.33	76.59		
Transect 1, loc. 1	119	0.2	3049	0.0	0.0	42.46	76.50	7	50
Transect 1, loc. 2	122	0.2	3660	1.0	1.0	42.46	76.50	6	70
Transect 1, loc. 3	122	0.3	5190	9.5	9.5	42.46	76.50	6	70
Transect 1, loc. 4	137	0.3	6720	24.0	24.0	42.46	76.50	7	20
Transect 1, loc. 5	162	0.2	5510	21.0	21.0	42.47	76.50	7	20
Transect 1, loc. 6	186	0.4	5510	12.0	12.0	42.47	76.50	7	20
Transect 1, loc. 7	229	0.8	22600	13.0	19.5	42.47	76.49	8	30
Transect 2, loc. 1	277	5.2	412195	7.5	3.2	42.46	76.44	8	30
Transect 2, loc. 2	287	5.4	461000	7.0	4.7	42.46	76.44	7	40
Transect 2, loc. 3	314	5.8	472000	5.5	5.5	42.45	76.43	5	70
Transect 2, loc. 4	378	6.3	514000	13.0	30.3	42.45	76.42	7	20
Transect 2, loc. 5	433	6.8	556000	4.0	6.0	42.45	76.42	5	50
Transect 2, loc. 6	430	7.9	558000	9.0	9.0	42.45	76.41	6	70
Transect 2, loc. 7	457	8.4	570000	9.0	9.0	42.46	76.40	7	30
Transect 2, loc. 8	469	8.7	581000	3.0	2.0	42.46	76.39	5	80
Transect 2, loc. 9	488	9.1	588000	7.0	4.7	42.46	76.39	7	30
Transect 2, loc. 10	530	9.6	612000	5.0	0.0	42.46	76.38	3	90
Transect 2, loc. 11	503	9.9	613000	8.8	8.8	42.46	76.38	4	70
Transect 2, loc. 12	491	10.1	614000	8.0	32.0	42.46	76.38	5	60
Transect 3, loc. 1	119	3.6	27439	0.0	0.0	42.43	76.51	5	90
Transect 3, loc. 2	119	3.8	30500	1.7	1.7	42.43	76.51	6	70
Transect 3, loc. 3	122	3.9	31300	15.0	15.0	42.43	76.51	6	60
Transect 3, loc. 4	168	4.2	42800	23.0	23.0	42.42	76.51	8	20
Transect 3, loc. 5	244	4.9	92400	8.5	8.5	42.42	76.51	7	30
Transect 3, loc. 6	280	5.4	128000	5.5	8.3	42.41	76.51	7	60
Transect 3, loc. 7	299	5.8	141000	5.0	3.3	42.41	76.51	6	50

Table 3. This extract of a larger data table provides an example of the weighting factors that were calculated to be able to compare transect locations to local stations (as here) or to nearby RAP-model gridpoints. These are the final (version 1) factors, thus being an average of tables comparing on the basis of similarity in geometric distance, elevation, and distance from the nearest point on Cayuga Lake as calculated from the metadata in Table 2.

	G.F. Rainwise	KNYTRUMA2	KNYITHAC15	KNYITHAC7	KNYITHAC1	KNYITHAC14	KNYITHAC12	KNYITHAC16	KITH	KNYDRYDE3	KNYDANBY1	KNYITHAC17
Transect 3, loc. 1	0.04	0.02	0.02	0.27	0.41	0.03	0.02	0.08	0.04	0.01	0.02	0.03
Transect 3, loc. 2	0.05	0.02	0.02	0.17	0.42	0.03	0.02	0.14	0.06	0.01	0.02	0.03
Transect 3, loc. 3	0.05	0.03	0.04	0.14	0.36	0.04	0.03	0.19	0.06	0.01	0.02	0.03
Transect 3, loc. 4	0.06	0.03	0.32	0.10	0.07	0.04	0.03	0.16	0.11	0.01	0.02	0.04
Transect 3, loc. 5	0.20	0.08	0.06	0.11	0.09	0.06	0.06	0.10	0.14	0.02	0.03	0.06
Transect 3, loc. 6	0.30	0.11	0.03	0.08	0.06	0.06	0.05	0.09	0.10	0.02	0.03	0.07
Transect 3, loc. 7	0.21	0.22	0.03	0.08	0.06	0.06	0.05	0.09	0.10	0.02	0.03	0.06

Works Cited

Froelich, N.J., and H.P. Schmid, 2006. "Flow divergence and density flows above and below a deciduous forest: Part II. Below-canopy thermotopographic flows." *Agricultural and Forest Meteorology*, Vol. 138, Issues 1-4. <http://www.sciencedirect.com/science/article/pii/S0168192306000967>

Georgakis, C. and M. Santamouris, 2006. "Experimental investigation of air flow and temperature distribution in deep urban canyons for natural ventilation purposes." *Energy and Buildings*, Vol. 38, Issue 4. <http://www.sciencedirect.com/science/article/pii/S0378778805001350>

Giovannini et. al., 2011. "Analysis of the Urban Thermal Fingerprint of the City of Trento in the Alps." *Journal of Applied Meteorology and Climatology*, Vol. 50 (5), 1145-1162. <http://journals.ametsoc.org/doi/abs/10.1175/2010JAMC2613.1>

Lahiff, Conor. National Weather Service, Burlington, VT. Personal communication. 12 September 2013.

Linacre, E., and B. Geerts. "Roughness Length." *University of Wyoming*. University of Wyoming. Apr. 1999. Accessed Dec. 5, 2013. <http://www-das.uwyo.edu/~geerts/cwx/notes/chap14/roughness.html>

Lookingbill, Todd R., and Dean L. Urban, 2003. "Spatial estimation of air temperature differences for landscape-scale studies in montane environments." *Agricultural and Forest Meteorology*, Vol. 114, Issues 3-4. <http://www.sciencedirect.com/science/article/pii/S016819230200196X>

Mahoney et. al., 2010. "Vehicles as Mobile Weather Observation Systems." *Bulletin of the American Meteorological Society*, Vol. 91 (9), 1179-1182. <http://journals.ametsoc.org/doi/abs/10.1175/2010BAMS2954.1>

Muller et. al., 2013. "Toward a Standardized Metadata Protocol for Urban Meteorological Networks." *Bulletin of the American Meteorological Society*, Vol. 94 (8), 1161-1185. <http://journals.ametsoc.org/toc/bams/94/8>

Niachou, K., I. Livada, and M. Santamouris, 2008. "Experimental study of temperature and airflow distribution inside an urban street canyon during hot summer weather conditions. Part II: Airflow analysis." *Building and Environment*, Vol. 43, Issue. 8. <http://www.sciencedirect.com/science/article/pii/S036013230700042X>

Pypker et. al., 2007. "Cold air drainage in a forested valley: Investigating the feasibility of monitoring ecosystem metabolism." *Agricultural and Forest Meteorology*, Vol. 145, Issues 3-4. <http://www.sciencedirect.com/science/article/pii/S0168192307001086>

Sedlák et. al., 2010. “Night-time airflow in a forest canopy near a mountain crest.” *Agricultural and Forest Meteorology*, Vol. 150, Issue 5. <http://www.sciencedirect.com/science/article/pii/S0168192310000377>

Sonne, Jeffrey K., and Robin K. Vieira, 2000. "Cool Neighborhoods: The Measurement of Small Scale Heat Islands." *Proceedings of 2000 Summer Study on Energy Efficiency in Buildings*, American Council for an Energy-Efficient Economy, 1001 Connecticut Avenue, Washington, DC. <http://www.fsec.ucf.edu/en/publications/html/FSEC-PF-363-01/>

Wang, Wenhui, Shunlin Liang, and Tilden Meyers, 2008. “Validating MODIS land surface temperature products using long-term nighttime ground measurements.” *Remote Sensing of Environment*, Vol. 112, Issue 3. <http://www.sciencedirect.com/science/article/pii/S0034425707003914>

Weather Underground. “About Our Data.” *Weather Underground.* 2014. <http://www.wunderground.com/about/data.asp>

Wood et. al., 2013. “An Overview of the Urban Boundary Layer Atmosphere Network in Helsinki.” *Bulletin of the American Meteorological Society*, Vol. 94, No. 11: pp. 1675-1690.